Wireless In-House Data Communication via Diffuse Infrared Radiation

FRITZ R. GFELLER AND URS BAPST

Abstract—A novel wireless broadcast/multi-access channel is described for flexibly interconnecting a cluster of data terminals located within the same room. The transmission medium is diffusively scattered infrared radiation at 950-nm wavelength. Transmission is low-to-medium speed and the range up to 50 m. Theoretical analysis indicates that the time dispersion limits the transmission bandwidth of the system to 260 Mbit · m/s, but background noise produced by ambient daylight reduces the transmission speed below 1 Mbit/s. The transmission properties of the diffuse optical channel are analyzed, and experimental digital links for baseband PCM at 125 kbit/s and PSK 64 kbit/s are demonstrated.

I. Introduction

WE ARE at present facing an enormous growth of computer-based terminal stations. These terminal stations are interconnected to form distributed or centralized computer networks of increasing complexity and density to perform a variety of functions. In the office environment, individual word processing, data processing, and information systems move towards integrated office systems. On the shop-floor level, process control, manufacturing, and testing depend increasingly on a multitude of interconnected terminal stations such as sensors, transducers, microprocessors, or industrial robots. Similarly, in the merchandising environment, cash-register terminals, stock taking, or order placements are becoming increasingly a part of common data-processing systems. This development has had an impact on the system architecture and a number of pertinent architectures has been conceived [1]-[3] with an end to flexibility and adaptation to growth.

In the same room or shop floor there is often a multitude of terminals clustered together. There is a need to flexibly place terminals at different positions within the same room to suit particular working conditions, to reconfigurate existing terminal arrangements, or even to have mobile hand-held terminals. Examples are cash-register terminals in supermarkets or data terminals in a production plant where economic production of a particular model requires frequent modifications in number and location of the terminals.

The conventional method of interconnecting terminals is by wiring. There is often a multitude of different cable types to suit particular transmission speeds. While mains powering is readily available and prewired with tapping points within easy reach, signal cables may have to be pulled individually. Actual situations are very diverse and difficult to categorize, but, in general, the cabling problem ranges from low-cost solutions of loose cables on the floor to crowded ducts or even raised floors with high costs. Once the cables have been installed, changes are costly and cause downtime. In addition, there may also be problems with ground loops and noise pickup.

Manuscript received February 8, 1979; revised June 22, 1979.

The authors are with the IBM Zurich Research Laboratory, Rüschlikon, Switzerland.

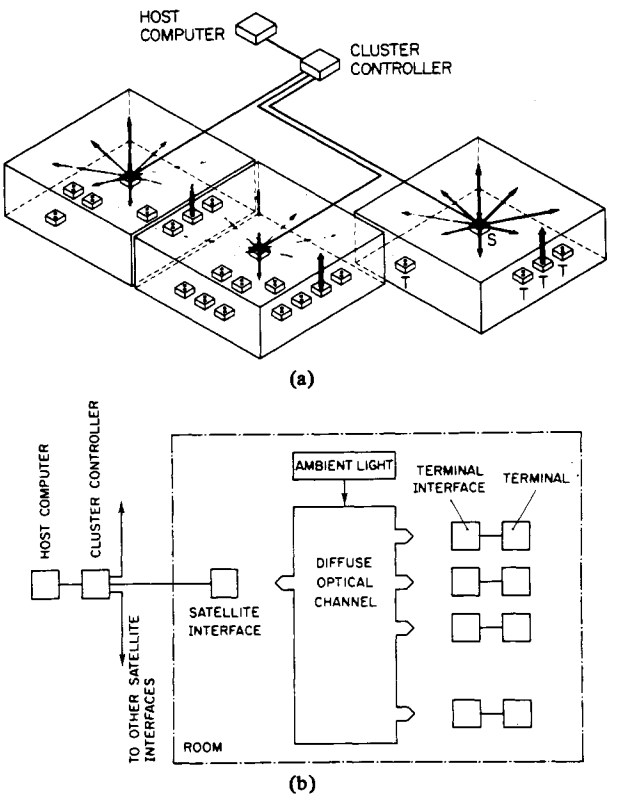

Fig. 1. (a) Diffuse optical channels connecting terminal clusters in an in-house environment. S = satellite, T = terminals. (b) Diffuse optical-channel network.

A. Wireless Optical Channel

An alternative to cabling is wireless communication. In this paper, we propose diffuse optical radiation in the near-infrared region as signal carrier to interconnect a cluster of terminals located in the same room to a common cluster controller [4]. In principle, each terminal interface is equipped with a light-emitting diode LED and a photodiode for converting an electronic signal to an optical signal, and vice versa, and the corresponding driver and receiver circuits. Similarly, a central optical satellite station serves as an interface to the common cluster controller which may be local or remotely connected via a conventional wire link (see Fig. 1(a)). Optical radiation from the satellite (downlink) is diffusely scattered from the surrounding walls, ceiling, and other objects in the room, thus filling the entire room with the optical signal carrier. Reception is nondirectional, i.e., the photodiodes receive the incoming

0018-9219/79/1100-1474$00.75

radiation from a wide field of view (FOV). Hence, there is no direct line of sight required between transmitter and receiver, and the optical transmission path is very insensitive to interruption. The same transmission method applies for the uplink (terminals to satellite).

A comparison between diffuse optical and radio-frequency transmission reveals the following aspects in favor of the optical link: with radio-frequency transmission FCC regulations apply within the range 10 kHz to 300 GHz. There are two classes, namely, licensed transmitters and unprotected restricted radiation devices. For the applications considered, licenses are obtained with increasing difficulty due to the overcrowded spectrum.

The optical signal carrier considered does not fall under FCC regulations and there is no interference with the electromagnetic spectrum. In contrast to radio-frequency antennae, the dimensions of LED and photodiodes are small, and the optical radiation is essentially confined to the room where it is generated. There is thus no interference with similar systems operating next door and a higher degree of data security is afforded than radio-frequency transmission can offer. An interesting possibility in connection with diffuse optical transmission is the operation of wireless hand-held terminals. Progress in low power-consumption microprocessors, liquid-crystal displays, and miniature keyboards has brought a battery-driven personal terminal within the state of the art [5], [6]. Conceivable applications are message transmission, paging, voice transmission, remote control, stock taking, or classroom teaching.

Since the appearance of the first LED there has been enormous progress in the technology of electrooptical components for optical communications. Of special importance to us are high radiant output, high efficiency LED's, sensitive large-area and low-capacity pin photodiodes, as well as low-noise optical receiver circuits. On the consumer market, wireless infrared devices have already made their mark in remote control of TV sets and earphones for audio transmission.

B. System Aspects

The diffuse optical channel can be visualized as a completely connected network (see Fig. 1(b)). Optical radiation from the satellite (downlink) reaches every terminal within the room, thus forming a broadcast channel. Since this channel is used only for the satellite, no collisions of data packets can occur. The terminals select only packets addressed to themselves and discard the rest. Radiation from the terminals reaches the satellite as well as the other terminals. (However, there may be "hidden" terminals not in contact with one another.) The uplink is thus a multi-access channel. Here, the problem of time sharing among all users arises. Access may either be random or by polling. The polling process may be based on an SDLC-type protocol where the cluster controller serves as a primary station. A performance analysis of various random access methods such as ALOHA or carrier-sense multiple-access CSMA has been given by Kleinrock *et al.* [7]. Data transmission may be either baseband PCM or by modulated carrier methods such as FSK or PSK. The carrier method offers the possibility of having several separate optical channels. The diffuse optical channel supports a large population of active and inactive users. In wire communications, the maximum number of users is often bounded by some hardware limitations. In wireless communications each user is represented by an address and the number of users is only bounded by channel capacity. There is no limit to temporarily inactive users beyond that of finite address field size. An in-house system based on diffuse optical channels may be expanded or contracted without major changes and offers great flexibility. A diffuse optical channel could also serve as a subnet in a local area network.

C. Overview of the Topics Addressed

In this paper, we present a study on the potential and limitations of the diffuse optical channel. Our effort has been concentrated mainly on the physical transmission properties, namely, bandwidth limitations due to multipath signal dispersion, optical power demand for satellite and terminal interfaces, as well as range and distribution of the diffuse optical radiation field.

In Section II, we describe an idealized diffuse optical channel. It can be visualized as a transmitter and receiver sitting in an optical cavity representing a room. If the cavity walls are uniformly illuminated by the transmitter then the optical signal power incident on the receiver photodiode is constant, irrespective of the location and orientation of the receiver within the cavity. This is a most desirable feature which, however, can only be approximated in practice. We also investigate the effect of multipath propagation within the cavity. The resulting time dispersion is analyzed assuming a signal which is diffusely reflected from a plane surface (ceiling). A bandwidth–distance product is then derived indicating an upper bound for the transmission speed for a given room size.

In Section III, a baseband PCM receiver is discussed both theoretically and experimentally. Apart from the infrared signal, the receiver photodiode is also exposed to ambient light. A photon striking the photodiode produces, with a given probability, a hole–electron pair which is manifested as an electrical current in the external circuit. Since this is a statistical process, the generation of the photocurrent due to ambient light is associated with noise which degrades the transmission quality. Some typical ambient-light levels in office environments have been measured and optical filters for blocking part of the ambient light are discussed. The optical receiver power required for a prescribed transmission error rate is then calculated with the ambient-light level and transmission speed as parameters. Finally, an experimental PCM receiver operating at 125 kbit/s is described. Measurements of the error performance showed good agreement with theory. However, with baseband receivers, transmission integrity may be impaired in the presence of fluorescent lamps emitting light with frequency components falling within the receiver passband.

Section IV addresses the infrared field distribution in a complex environment. A brief survey of the infrared reflective properties of office interiors is given. A computer model is then described simulating the distribution of the diffuse infrared field for a given room geometry and transmitter LED configuration. With the aid of this simulation model, suitable LED configurations can be found that provide a sufficiently uniform illumination of a given interior. A case study of three different room geometries and satellite LED configuration is then presented. Finally, using the above three cases as an example, the optical power needed for a 64-kbit/s link is estimated for both the satellite interface and the terminal interfaces.

Section V deals with an experimental 64-kbit/s PSK transmitter–receiver interface using a 256-kHz carrier. The use of a

carrier allows operation of several separate channels. Furthermore, the receiver passband is shifted away from the baseband, thus allowing effective electrical filtering of ambient-light fluctuations.

II. Idealized Diffuse Optical Channel

A. Optical Power Received from Diffusely Reflecting Surface

The key features of the diffuse optical channel are readily derived from a simple idealized model. An optical source illuminates an arbitrarily shaped surface A such that the radiant emittance w (power emitted per surface area into hemisphere) is constant over the entire area A (see Fig. 2). We further assume that the surface is an ideal Lambertian reflector. A photodiode with photosensitive area A_R and field of view FOV is then subject to the diffusely scattered radiation from surface A. The system optical source (satellite), a cavity with diffusely reflecting surface A (representing the physical bounds of the room), and the photodetector (terminal) thus form a diffuse optical channel. The optical power incident on the photosensitive area A_R from the surface element dA is given by

$$dP_R = \frac{1}{\pi} w \cos\gamma \, dA \, d\Omega \tag{1}$$

where

$$d\Omega = \frac{1}{R^2} A_R \cos\delta, \quad \text{if } A_R \ll R^2$$

$$dA = \frac{1}{\cos\gamma} R^2 \sin\delta \, d\delta \, d\epsilon.$$

All variables are functions of the coordinates δ and ϵ. If we consider only a homogeneously illuminated surface A with w a constant, then the total power incident on A_R is obtained by integrating over the entire FOV

$$P_R = \frac{w}{\pi} A_R \int_0^{\text{FOV}} \int_0^{2\pi} \sin\delta \cos\delta \, d\delta \, d\epsilon \tag{2}$$

and

$$P_R = w A_R \sin^2(\text{FOV}), \quad 0 < \text{FOV} \leqslant 90^\circ. \tag{3}$$

Thus the received optical power P_R is independent of position and angular orientation of the photodetector with respect to the surface A, provided the surface covers the entire FOV. A hypothetical but illustrative example is a spherical cavity illuminated by an isotropic source located in the center. An estimate of the optical-power demand P_s for the source illuminating the cavity wall A is given by

$$P_s \cong \frac{A P_{\min}}{A_R \rho \sin^2(\text{FOV})} \tag{4}$$

where $P_{\min}$ is the minimum power required by the receiver circuit, and ρ is a reflection coefficient indicating the proportion of diffusively reflected incident radiation.

The theoretical minimum power P_{so} to supply a population of photodetectors arranged over a floor area A_F is given by

$$P_{so} = P_{\min} \frac{A_F}{A_R} \tag{5}$$

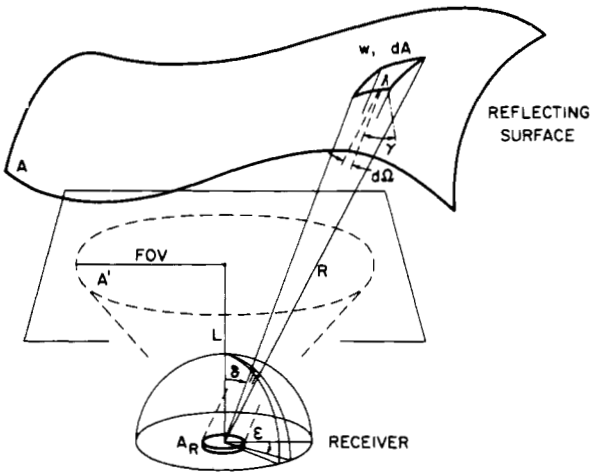

Fig. 2. Optical power received from diffusely reflecting surface.

where $\rho = 1$ and FOV $= 90^\circ$. This would require that the photodetectors be in close contact with the radiating surface $A = A_F$. Note that P_{so} is also the power contained in direct line-of-sight radiation from a distant source falling normally upon the area A_F.

The problem in a real environment will therefore be to distribute the source radiation to the reflecting surfaces as homogeneously as possible, bearing in mind their size, geometry, and reflective properties, in order to achieve an approximately constant received signal power level over the entire working area of the room.

The photodiode represents a relatively high-cost high-capacitance device with area A_R where the incident radiation is collected and converted to an electronic signal. Therefore, it appears attractive to collect optical radiation with a low-cost passive optical system (lenses, reflectors) having a large aperture A_L and concentrating the incident radiation on a small-area low-capacitance photodiode. However, from phase-space [8] or second-law thermodynamic considerations [9] it has been shown that three-dimensional ideal concentrators obey the relation

$$A_R = A_L \sin^2(\text{FOV}). \tag{6}$$

Hence, there is no gain possible over a single photodiode exposed to a homogeneously radiating surface A extending over the full hemispherical FOV. Furthermore, practical concentrating systems resemble the theoretical performance for relatively small angles FOV $\leqslant 30^\circ$ only. This is already a constraint on the freedom of angular position of the photodiode with respect to the environment. For these reasons, passive optical systems appear only to be useful for direct line-of-sight transmission, for bounded diffusely reflecting areas appearing below an angle smaller than 30°, or if a bright ambient-light source is to be kept out of the FOV.

B. Multipath Dispersion

We now consider the effect on signal distortion due to multipath propagation. In order to gain a simple representative result, the reflecting surface A of arbitrary shape is replaced by a plane surface A' (ceiling) with distance L from the photodiode (see Fig. 2). At time $t = 0$ a Dirac pulse arriving from a distant source is reflected by the surface A', producing an impulsive uniform radiant emittance w over the entire surface. The optical power incident on the photodiode at the propaga-

tion delay τ is, using (1) and expressing R in terms of τ,

$$dP_R(\tau) = 2wA_R\tau_0^2 \frac{1}{\tau^3}\, d\tau, \qquad \tau_0 \leqslant \tau \leqslant \frac{\tau_0}{\cos(\mathrm{FOV})} \tag{7}$$

where

$$\tau = \frac{L}{c\cos\delta}$$

$$\tau_0 = \frac{L}{c}.$$

Here, c is the speed of light and τ_0 the minimum delay. The contribution $dP_R(\tau)$ within the time element $d\tau$ originated from annular surface elements dA'. From (7), the normalized impulse response $F(\tau)$ is calculated using (7) and (3)

$$F(\tau) = \frac{dP_R}{P_R d\tau} = \begin{cases} \dfrac{2\tau_0}{\tau^3 \sin^2(\mathrm{FOV})}, & \tau_0 \leqslant \tau \leqslant \dfrac{\tau_0}{\cos(\mathrm{FOV})} \\ 0, & \text{elsewhere.} \end{cases} \tag{8}$$

Bearing in mind the impulse response, the resulting normalized signal pulse shape $g(t)$ arriving at the photodiode may be obtained by convoluting $F(\tau)$ with the original signal $f(t)$ incident on the reflecting surface

$$g(t) = \int_{-\infty}^{\infty} f(t-\tau)\, F(\tau)\, d\tau \tag{9}$$

where

$$\int_{-\infty}^{\infty} F(\tau)\, d\tau = 1$$

$$\int_{-\infty}^{\infty} f(t)\, dt = 1$$

$$\int_{-\infty}^{\infty} g(t)\, dt = 1.$$

In Fig. 3, the impulse response $F(\tau)$ and the resulting pulse shape $g(t)$ for a rectangular pulse $f(t)$ of duration $T_D = L/c$ is given with FOV as parameter. Multipath propagation causes a spread of the transmitted pulse which may result in a loss of pulse amplitude and intersymbol interference. There is, therefore, a maximum transmission speed ultimately depending on room size, where these effects affect transmission if no signal processing is used. In a given environment, the multipath conditions are somewhat different for each source/receiver configuration. However, an example shall serve as a rough estimate for the maximum transmission speed with baseband transmission. Consider source and receiver located at the same position at some distance L from the reflecting surface which may represent the ceiling of a large room. The radiation characteristics of the source are assumed to cause a homogeneous radiant emittance w of the surface appearing within the circular FOV of the receiver. Assuming rectangular pulses $f(t)$ with 50-percent duty cycle and FOV = 60°, the above-mentioned criteria for zero amplitude loss and intersymbol interference of the received pulses $g(t)$ are just met (see Fig. 3). Here, we

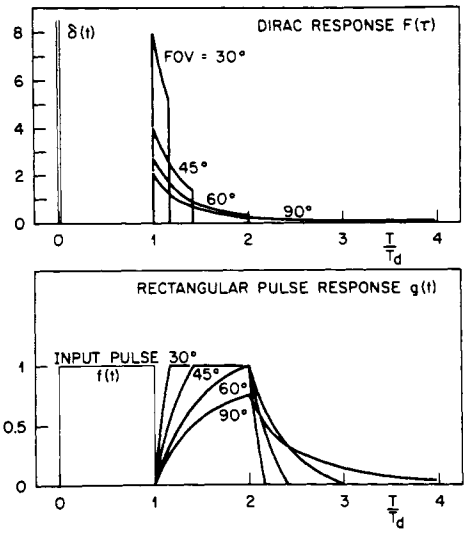

Fig. 3. Signal dispersion due to multipath propagation. The top figure shows the impulse response of a plane diffusely reflecting surface. The bottom figure shows the corresponding rectangular pulse response.

have to consider a double propagation delay to account for the individual source-to-reflector and reflector-to-receiver paths. We can approximately associate the circular area in the reflecting surface, as described by the FOV, with the room size. For a diameter of 5 m (small room) the transmission speed satisfying the above criteria is 52 Mbit/s. Similarly, for a diameter of 50 m (hall) the transmission speed is still 5.2 Mbit/s. This result may be expressed in terms of a bandwidth-distance product amounting to approximately 260 Mbitm/s. These speeds are sufficient for local data distribution. However, if a modulated carrier is used these considerations apply to the carrier frequency to limit phase distortions.

III. Optical Receiver

A. Ambient Light

In a diffuse optical channel, the photodiode is exposed to the ambient light, introducing additional noise to the input circuit of the receiver amplifier. This is in contrast to fiber-optics receivers. The most commonly encountered ambient-light sources are daylight, tungsten, and fluorescent lamps. Their relative spectral power densities are shown in Fig. 4. In general, there is a high level of stationary or slowly fluctuating ambient light generating shot noise in the photodiode. In addition, artificial-light sources also emit rapidly fluctuating components associated with higher harmonics of the mains frequency. These have to be eliminated by electrical filtering. Part of the incident ambient light may be blocked by an optical filter (see Fig. 4). Two types of filters may be used: optical interference filters with a passband corresponding to the LED source bandwidth (with due allowance for nonnormal incidence) and absorption edge filters blocking only the visible part of the spectrum. An effective and inexpensive filter is obtained by developing an unexposed color film. Due to the different source spectra, the filter is able to block ambient light to a varying degree of effectiveness [10]. The transmission is approximately 1 percent at 720 nm and 85 percent at the LED wavelength of 950 nm. Even for the proposed indoor use of the transmission system, the ambient-light level varies over several orders of magnitude. A series of measurements has indicated some typical ranges (see Fig. 5). The intensities

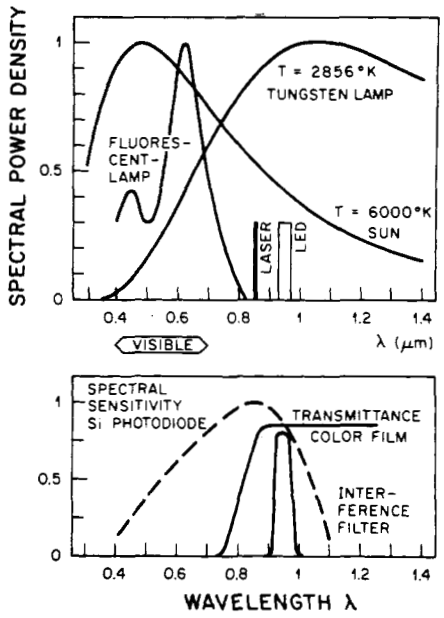

Fig. 4. Spectral power density of three common ambient-light sources. The bottom figure shows the effect of two different optical filters.

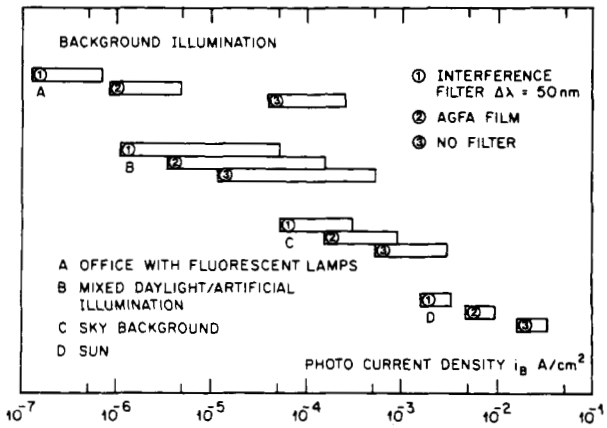

Fig. 5. Photocurrent density of typical ambient-light environments. Measurements taken with a 1-cm² pin Si-photodiode and 50° FOV.

are given in terms of photocurrent density i_B rather than radiometric units to avoid referring to the different spectra. The approximate blocking effects of the filters are also shown. The ambient-light level determines, to a significant degree, the optical signal power required for reliable transmission. For reference purposes, we have considered two particular ambient-light environments.

In a predominantly daylight environment we chose $i_B = 1.5 \times 10^{-4}$ A/cm², using a color film as filter. This value corresponds to approximately 380 Lux and was measured near windows but with the photodiode not exposed to direct sunlight. The same photocurrent density is also obtained with the photodiode placed under a 75-W tungsten desk lamp at 65-cm distance. Alternatively, in a well-lit windowless room with fluorescent lighting, the resulting photocurrent density is $i_B = 3 \times 10^{-6}$ A/cm² corresponding to 200 Lux in photometric units.

B. Required Optical Receiver Power

We shall now calculate the input optical power required by the receiver in the presence of stationary ambient light. In principle, baseband PCM or carrier-modulated transmission

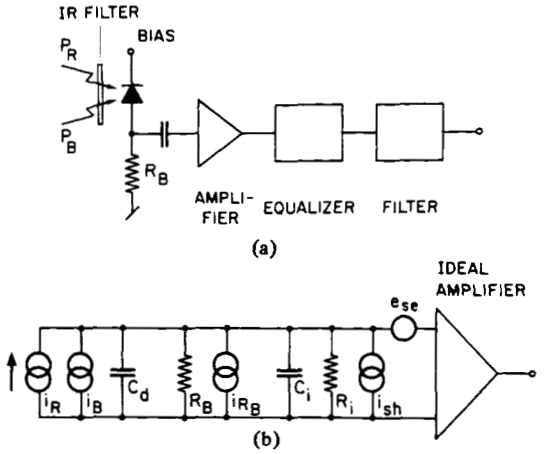

Fig. 6. (a) Block diagram of PCM baseband receivers. (b) Noise equivalent circuit diagram.

may be used. In the literature, extensive work has been published by Goell [11] and Personick [12] on baseband PCM fiber-optics receivers, and we shall follow their approach. The noise equivalent receiver circuit diagram is shown in Fig. 6. The minimum average optical power $P_{\min}$ is given by

$$P_{\min} = \frac{h\nu}{\eta e} Q \left[\overline{i_{\text{eff}}^2}\right]^{1/2} \tag{10}$$

where Q is a function of the error probability p_e

$$Q = \sqrt{2}\ \text{erfc}^{-1}\ (2p_e) \tag{11}$$

and the effective noise current is

$$\overline{i_{\text{eff}}^2} = 2eI_B f I_0 + 4kTf \frac{R_B g_m + \Gamma}{R_B^2 g_m} I_0 + \frac{8kTf(2\pi f C_D)^2}{3g_m} I_2. \tag{12}$$

Here, h is Planck's constant, η the photodiode quantum efficiency, ν the optical frequency, e the charge of an electron, T the temperature; $I_0 = 0.3$ and $I_2 = 0.13$ are shape factors for 50-percent duty-cycle signal pulses, and f is the bit rate. For the Si-FET input stage the transconductance is $g_m = 0.005$ mho and the noise multiplication factor is $\Gamma = 0.66$ [13]. C_D and R_B are the photodiode capacitance and bias resistance, respectively. They both dominate the other input capacitances and resistances for the application considered. The first term of (12) describes the shot noise generated by the stationary photocurrent I_B due to ambient light. The remaining terms represent thermal and amplifier noise. In principle, the bias resistor R_B should be made large to reduce thermal noise, but this requires an equalizer to compensate for the signal distortion introduced by the input circuit with time constant $T_D = R_B C_D$. Proper equalization with $T_D \gg 1/f$, where f is the bit rate, requires careful adjustment. However, the diode capacitance does not remain constant because of fluctuations of the bias voltage caused by the ambient-light photocurrent. We therefore consider two cases, one with modest equalization $T_D = 1/f$, and with $R_B = 50\ \Omega$, where the latter does not require equalization for the bit rates considered. The signal photocurrent I_R increases proportionally with the photodiode area A_R, whereas the shot-noise current I_B increases with $\sqrt{A_R}$. An overall gain in signal-to-noise ratio is therefore expected for large-area photodiodes. Combining (3) with (10)

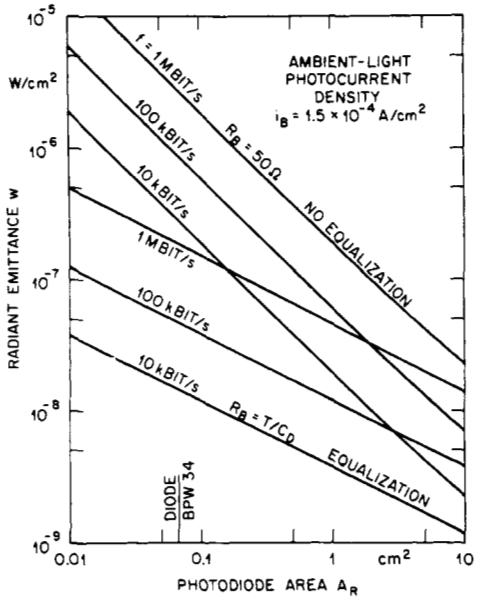

Fig. 7. Required radiant emittance of the diffusely reflecting environment.

we obtain an expression for the required radiant emittance w of the reflecting surface

$$w = \frac{h\nu}{\eta e A_R \sin^2 (\text{FOV})} Q \left[\overline{i_{\text{eff}}^2}\right]^{1/2}. \qquad (13)$$

The receiver photodiode thus collects sufficient optical power if it *sees* a surface reflecting the infrared signal with a power density given by w. With a knowledge of the radiant emittance w, the optical transmitter power can be estimated by multiplying w with the total surface A of the cavity, bearing in mind the reflection coefficient ρ. Note that this method only applies for the case where the transmitter LED array is able to produce an approximately uniform illumination of the surrounding walls and ceiling. For numerical results, we assume the following parameters: the photodiode capacitance is $C_D = \alpha A_R$, where $\alpha = 200$ pF/cm², and the ambient-light photocurrent is $I_B = i_B A_R$, where $i_B = 1.5 \times 10^{-4}$ A/cm². The projected error probability is 10^{-9} ($Q = 6$), and FOV = 90°. In Fig. 7, the required radiant emittance is calculated as a function of the diode area A_R. The total photodiode area may be obtained by smaller photodiodes connected in parallel.

The equalized receiver circuit with $T_D = R_B C_D$ is dominated by ambient-light shot noise, whereas the low-impedance circuit is dominated by thermal noise from the bias resistor R_B. Note that the numerical value of w for the diffusely reflecting surface also corresponds to the power density of direct radiation with normal incidence. In comparison to the fiber-optics receiver a higher optical input power is required to compensate for the ambient-light shot noise.

C. Experimental Baseband PCM Receiver

We have measured the transmission error probability with an experimental baseband PCM receiver at $f = 125$ kbit/s. The diagram of the receiver circuit is shown in Fig. 8. The circuit is provided with automatic gain control AGC, internal clock extraction, and code conversion from RZ to NRZ. The transmission is coded diphase which facilitates clock extration and allows fixed threshold detection. Furthermore, the signal power spectrum [14] of coded diphase is zero at $f = 0$ which allows the introduction of a high-pass filter to attenuate low-frequency components from ambient-light fluctuations.

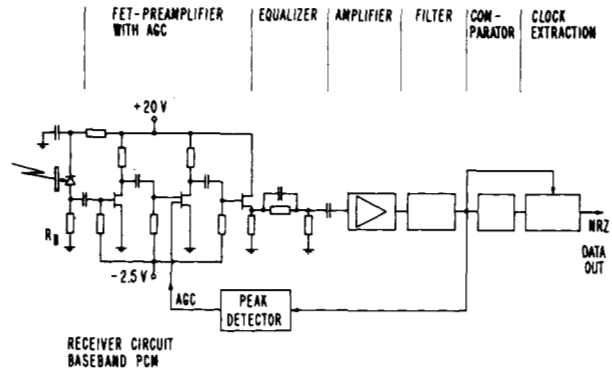

Fig. 8. PCM baseband receiver circuit.

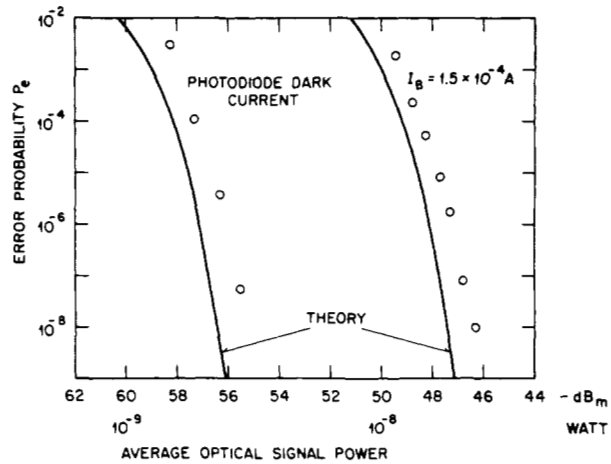

Fig. 9. Theoretical and experimental transmission error performance. Baseband PCM, $f = 125$ kbit/s.

For the measurements, the receiver is equipped with a large-area photodiode $A_R = 1$ cm² (type UDT PIN-10D). The measured diode capacitance is $C_D = 270$ pF, with $R_B = 31.6$ kΩ to form the time constant $T_D = 1/f$, and the quantum efficiency is $\eta = 0.57$ at $\lambda = 900$ nm. The stationary ambient-light photocurrent is $I_B = 1.5 \times 10^{-4}$ A corresponding to a photometric illumination of approximately 380 Lux.

The high-pass filter is formed by a cascade of 5-RC coupling circuits between amplifier stages and provides an asymptotic 100-dB/decade rolloff. The 3-dB point is chosen at 1.25 kHz which does not affect the quality of the eye pattern. The resulting error performance is shown in good agreement with the theory (see Fig. 9). However, in the vicinity of fluorescent lamps, additional transmission errors occur due to the presence of high-frequency components. Baseband PCM transmission is therefore vulnerable to rapid ambient-light fluctuations. A much higher rejection of ambient-light fluctuations can, however, be achieved with modulated carrier transmission.

IV. Diffuse Optical Channel

A. Simulation Model

A real office room or shop-floor environment represents a complex cavity with a variety of features such as geometry, size, and reflective properties. In order to establish guide lines for the design of hardware components we describe a computer model simulating the basic features. Of particular interest will be the optimization of the LED arrays to produce an economic

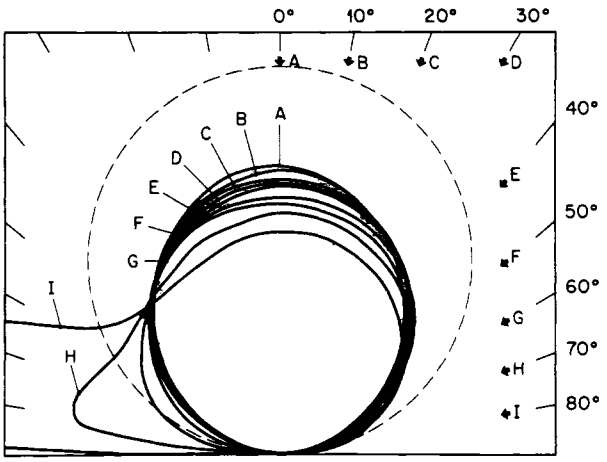

Fig. 10. Diffuse reflection polar diagram of a plaster wall. The letters indicate the angle of the incident-plane wave radiation. $\lambda = 950$ nm. The dotted circle represents an ideal Lambertian diffuser.

and relatively homogeneous diffuse radiation field over the whole floor area with respect to a given environment.

The transmission relies on efficient scattering of the incident LED radiation from the surrounding surfaces forming the structural environment of the room. We have made rough measurements of the reflection coefficient ρ at $\lambda = 950$ nm for a variety of commonly used materials: painted surfaces, wood panes, textiles, and plaster walls. Here, the reflection coefficient ρ is defined as the ratio of total power reflected into the hemisphere to plane wave incident radiation. We found that most of these materials reflect infrared radiation to 40–90 percent. The reflection characteristics are generally composed of a diffuse and a specular component, the latter becoming significant for very shallow angles of the incident radiation. Fig. 10 shows the polar scattering diagrams of a white plaster wall for different angles of incidence. Typical values of ρ for plaster walls have been found to vary between 0.7–0.85, depending on surface texture and angle of incidence, and the radiation characteristics are a close fit to a Lambertian distribution. Conclusively, most environments exhibit sufficiently good to excellent reflective properties for our purpose.

We now formulate the simulation model. The basic source element for the optical radiation consists of an LED. The angular distribution of radiant output power (radiation characteristics) is modeled with a generalized Lambert law

$$dP_n = \frac{n+1}{2\pi} \cos^n \alpha P_s \, d\Omega \tag{14}$$

where

$$P_s = \int_{\text{Hemisphere}} dP_n.$$

Here, P_s represents the total power radiated by the LED, dP_n is the power radiated into the solid angle $d\Omega$, n is a number describing the shape of the radiation characteristics, and α is the polar angle. With an epoxy lens attached to the LED housing, various radiation characteristics may be realized. The angular spread of the beam is indicated by the half-power angle α_H, where the intensity drops by a factor of 2

$$\alpha_H = \cos^{-1} (0.5)^{1/n}. \tag{15}$$

In practice, half-power angles down to $\alpha_H \cong 4°$, with $n = 300$, may be achieved with simple molded epoxy lenses. Fig. 11

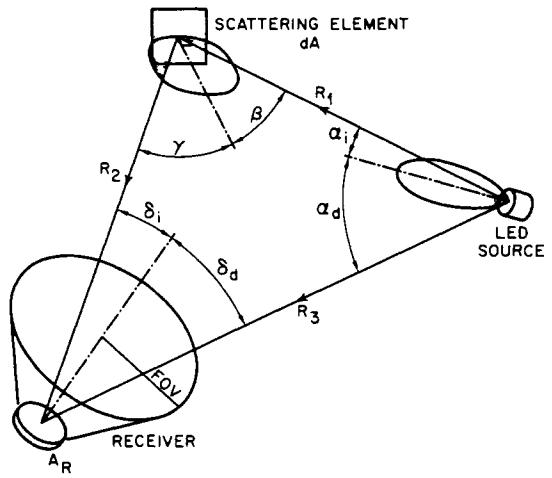

Fig. 11. Simulation model of the diffuse optical channel.

illustrates the gist of the diffuse optical-channel model. The power dP_n radiated by the LED into the solid angle $d\Omega$ is incident on the surface element dA from where a part dP_A is diffusely reflected with a Lambert distribution. The resulting radiant emittance w of the surface element is then given by

$$w = \frac{dP_A}{dA} = \frac{n+1}{2\pi R_1^2} P_s \rho \cos^n \alpha_i \cos \beta \tag{16}$$

where

$$d\Omega = \frac{dA}{R^2}, \qquad R^2 >> dA.$$

Hence, the power dP_A received from dA by the photosensitive area A_R is

$$dP_R = w \frac{A_R}{R_2^2 \pi} \cos \gamma \cos \delta_i \operatorname{rect} (\delta_i) \, dA \tag{17}$$

where

$$\operatorname{rect} (\delta_i) = \begin{cases} 1, & \text{if } |\delta_i| \leqslant \text{FOV} \\ 0, & \text{if } |\delta_i| > \text{FOV}. \end{cases}$$

The function rect (δ_i) describes the FOV of the photosensitive area which may be limited by a lens or an aperture to shield excessive ambient light. The total power received by diffuse reflection is then obtained by integrating over the entire reflecting area A and by summing over all LED sources. In symbolic notation

$$P_R = \sum_{\text{sources}} \frac{n+1}{2\pi^2} P_s \int_{\text{cavity walls}} \rho \cos^n \alpha_i \cos \beta \cos \gamma \cdot \cos \delta_i \operatorname{rect} (\delta_i) \frac{A_R}{R_1^2 R_2^2} \, dA. \tag{18}$$

As a first approximation, we have only considered single reflections. Similarly, the radiation incident on A_R via direct line of sight is

$$P_{Rd} = \sum_{\text{sources}} \frac{n+1}{2\pi} P_s \cos^n \alpha_d \cos \delta_d \operatorname{rect} (\delta_d) \frac{A_R}{R_3^2}. \tag{19}$$

Numerical results are obtained with a computer program calculating the optical signal power received as a function of position and angular orientation of the photodiode. The pro-

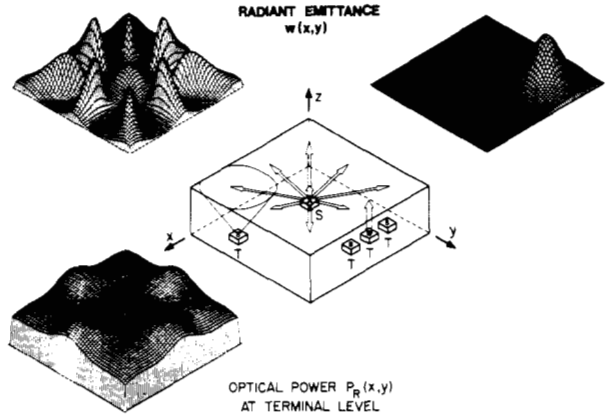

Fig. 12. Distribution of diffuse optical radiation in an office room environment. The plot in the upper-left corner shows the radiant emittance of the ceiling as produced by the satellite Sat. with a source array of nine LED's. The upper-right plot shows the radiant emittance produced by a terminal T with a Lambertian LED. The lower plot indicates the resulting received optical power (downlink) as a function of the terminal position. $S = 10$ m, $H = 3$ m, FOV = 90°, nondirectional case.

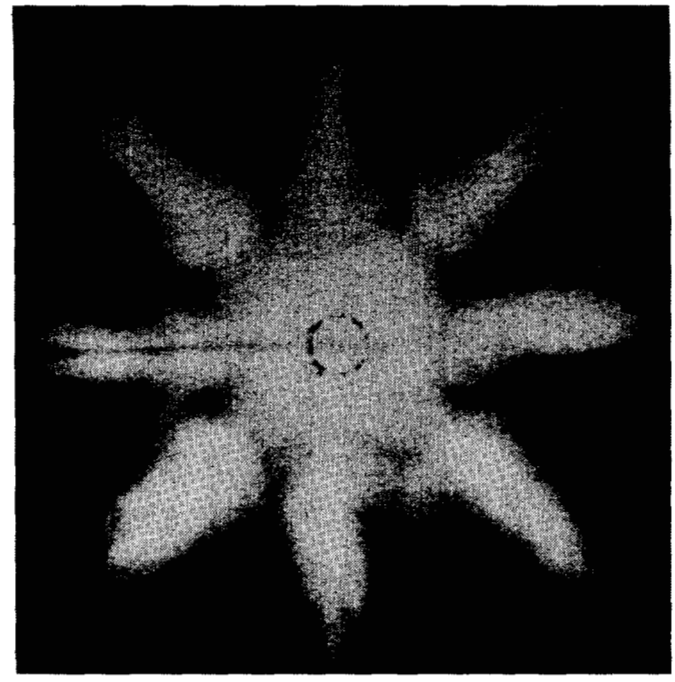

Fig. 13. Infrared spotlight pattern on diffusely reflecting surface. Image convertor photograph. The source consists of nine LED arrays. The irregularities of the individual LED radiation lobes are caused by manufacturing tolerances.

gram operates with the following parameters: the reflecting enclosure is defined as a rectangular box where each face may have a different reflection coefficient. The optical source parameters are represented by the positional coordinates (x_S, y_S, z_S), the orientation of the radiation axis, the emitted power P_S, and the shape factor n of the radiation lobe. Any number of different LED's may be simulated to form complex arrays. The receiver parameters are the positional coordinates (x_r, y_r, z_r), the orientation of the photodiode axis (normal to the photosensitive area A_R), and the FOV. Fig. 12 shows example plots of the radiant emittances generated by the satellite and terminal LED arrays, and of the resulting optical power received as a function of the terminal position. Fig. 13 shows the photograph of a scaled-down version of a spotlight pattern at the ceiling as produced by an array of LED's. Measurements of the diffuse radiation distribution produced with LED arrays in a scaled model environment have shown good agreement with the theoretical model.

B. Case Study: Three Types of Environment

We now discuss three examples of the downlink radiation distribution. The first two are simulated office room environments with dimension $S \times S \times H$, where S is the room size (length) ranging from 5 to 30 m, and $H = 3m$ is the height. The reflection coefficient of one side wall is set to zero to study the effect of a gross inhomogeneity of the environmental reflective properties such as a window facade. Glass panes reflect only specular images of the source where the reflection coefficient is determined by the Fresnel equations. With normal incidence the reflection is only about 5 percent and represents a direct line-of-sight link which may easily be blocked. The reflection coefficient of all other surfaces is assumed $\rho = 0.7$ (plaster walls and ceiling). All terminal photodiodes are located on desk level with $z_S = 1$ m. The coordinates x_S and y_S are variables, and FOV = 90°. We consider two angular orientations of the photodiodes. The first one is with the photosensitive surfaces parallel to the ceiling (nondirectional case). In this case the hemispherical FOV receives scattered radiation from all walls and the ceiling. In the second case, the photodiodes are tilted towards the center of the room (semidirectional case). Here, the normal axes to the photosensitive surface meet at a common fix point with coordinates ($S/2$, $S/2$, 6 m) and most radiation is received from the ceiling. The position of the satellite LED arrays is assumed to be in the center with coordinates ($S/2$, $S/2$, 1.5 m).

We first consider a satellite with a simple Lambert source. The axis of the radiation characteristics is normal to the ceiling. Fig. 14 shows the received signal power in function of the positional coordinates of the photodiodes for room sizes of $S = 5$ m to $S = 15$ m. The calculations were performed for both the nondirectional and semidirectional cases. The dB values indicate the variation encountered between maximum (center) and minimum (corner) signal power received.

The plots show that for rooms with an aspect ratio S/H close to unity, walls and ceiling are irradiated uniformly resulting in a smooth distribution of the signal power received. Position and orientation of the source have little influence. With increasing room size S most of the radiant emittance is concentrated at the center of the ceiling. Also, the effective projected area A_R of the receiving photodiodes becomes smaller with increased distance from the center. Considering a Lambertian source and the given room geometry with a low room height ($S = 3$ m), the maximum room size is limited to $S = 10$ m to 15 m. With larger sizes the variation of the signal power received with position becomes excessive. Our criteria for the variation allowed is the economic use of optical-source power and simple AGC in the receiver circuit.

For large office rooms an LED array with nine sources has been investigated. Here, the ceiling represents the main reflecting surface. Narrow beams from the LED array spotlight the ceiling in a regular pattern, thus transporting the signal power with little divergence. The spotlights act as secondary sources with Lambertian radiation characteristics, which in turn scatter the optical radiation at the predetermined location at some distance from the main source. Low partition walls or shelves separating individual work stations do not interfere with the

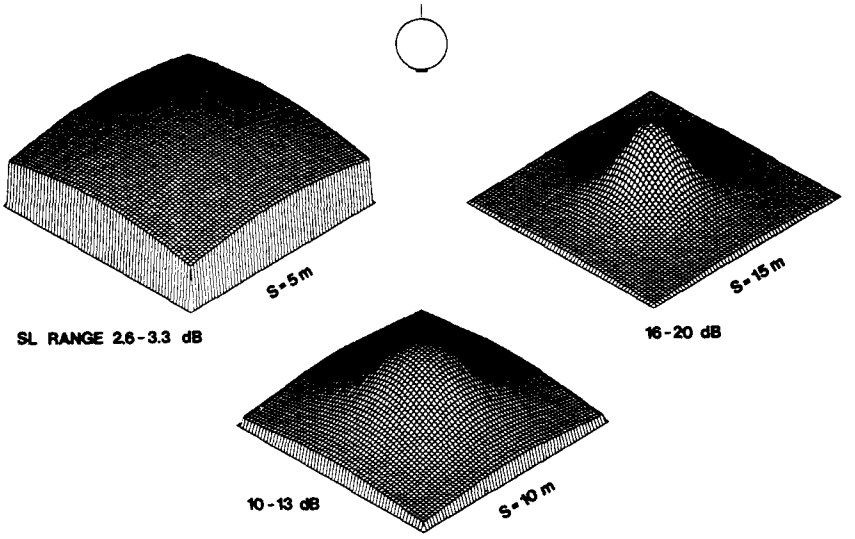

Fig. 14. Small office room. Received optical power as a function of terminal position. The dB figures indicate the encountered signal power variations for the semi- and nondirectional cases, respectively. The symbol indicates the Lambertian source. Plots refer to photodiodes in semidirectional orientation. FOV = 90°; room geometry $S \times S \times 3$ m.

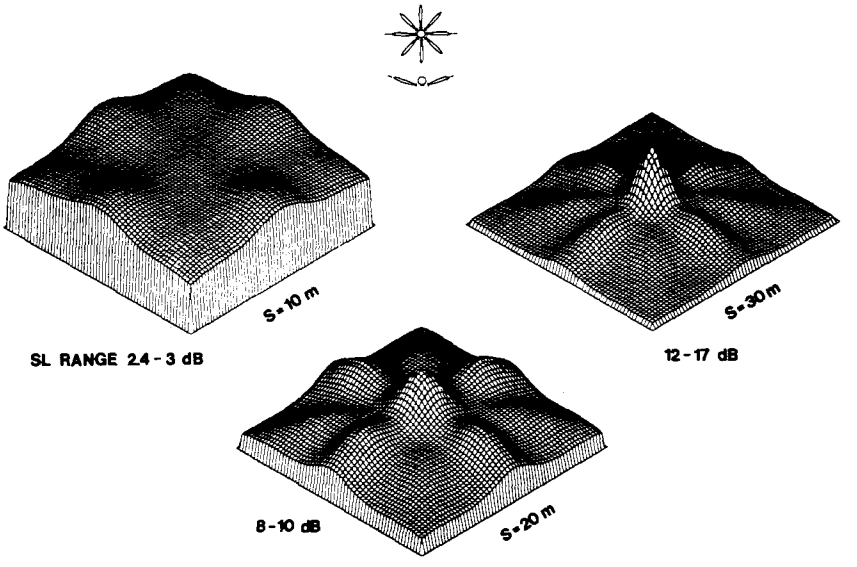

Fig. 15. Large office room. Received optical power as a function of terminal position. The dB figures indicate the encountered signal power variations for the semi- and nondirectional cases, respectively. The satellite source consists of eight LED's with $n = 100$, and one LED with $n = 1$. The location of the window front ($S = 1$) corresponds to the side marked with the room size S. Plots refer to photodiodes in nondirectional orientation. FOV = 90°; room geometry $S \times S \times 3$ m.

transmission as long as the FOV is sufficiently large. In Fig. 15, the plots of the signal power received as a function of the room size S show a more uniform distribution. With the array described a limit is reached at approximately $S = 30$ m, where the signal-power variation of 12–17 dB is exaggerated due to the central spotlight which is emphasized too strongly in comparison with the intensity of the sidelobes.

So far the angular orientations of the photodiodes have been assumed fixed. We are now interested in knowing the angular range within which sufficient optical power is received. Especially for hand-held terminals, it is important that the operation is not subject to severe angular and positional constraints. Fig. 16 shows calculated polar diagrams of the optical power received for three extreme locations A, B, and C within a room with $S = 20$ m. The polar diagrams indicate a rotation of the photodiode axis (normal to the photosensitive surface) by 180° about the coordinate axes x and y. The reference value 0 dB represents the minimum optical power required for a given transmission error rate. The total satellite power is adjusted so that at location C the power received in the nondirectional case (photodiode axis 90° elevation) reaches 0 dB. At location B the optical power received is a maximum, whereas at location C it is a minimum. The polar diagrams show that, apart from location along the window facade, the photodiode orientation may cover the full hemisphere. This feature has been confirmed by experimental tests.

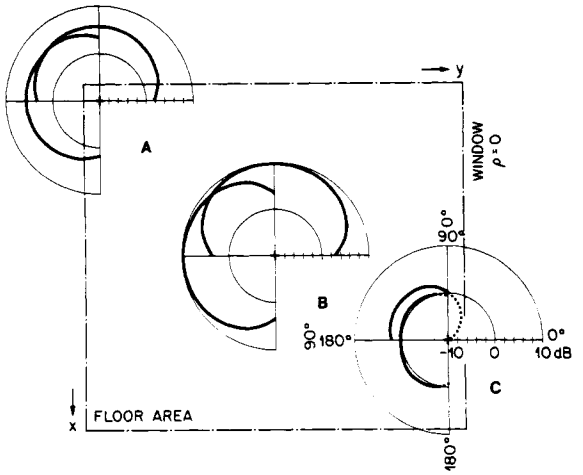

Fig. 16. Received optical power versus angular orientation for three specific terminal locations. The polar diagrams indicate P_R/P_{min} (dB). S = 20 m; FOV = 80°.

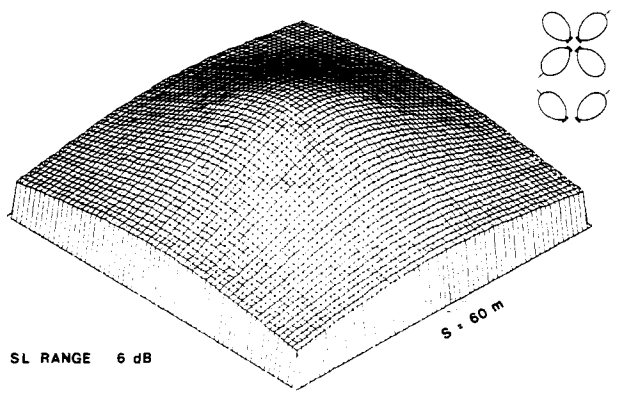

Fig. 17. Hall. Received optical power as a function of terminal position. There is little difference between semi- and nondirectional photodiode orientation. Satellite source consists of four LED's with n = 3. FOV = 90°; room geometry $S \times S \times S/4$.

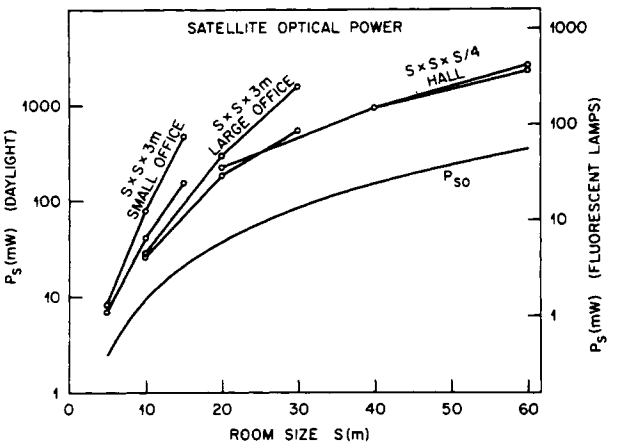

Fig. 18. Satellite optical power as a function of room size and geometry. Transmission speed f = 64 kbit/s. P_{SO} represents the theoretical minimum power for plane wave radiation.

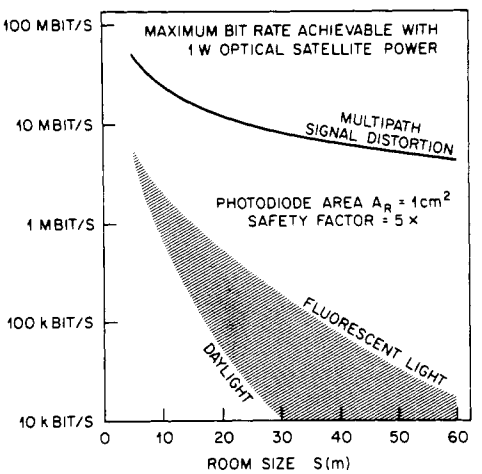

Fig. 19. Transmission speed versus room size.

Finally, we consider a hall with dimensions $S \times S \times S/4$. Here, the aspect ratio S/H is fixed. Due to the favorable geometry a simple LED array with four lobes provides a relatively uniform power distribution (see Fig. 17). Because of scaling, the power variation remains approximately constant for all sizes S.

C. Optical Satellite Power

We now estimate the total optical satellite power required for the previous example environments. The transmission speed assumed is 64 kbit/s and the receiver area A_R = 1 cm². From (10) the receiver power required for a transmission error rate $p_e = 10^{-9}$ is then p_{min} = 9.6 nW for daylight, and P_{min} = 1.5 nW for fluorescent ambient light, respectively, and $R_B = T/C_D$. Assuming constant ambient light, we obtain the total satellite power by equating the received power P_R, equation (18), at the position where the minimum occurs with the required power P_{min}. Hence, at this position, the power received from the satellite via diffuse reflections is just sufficient to establish the signal-to-noise ratio Q required for the transmission error rate prescribed. For all other terminal positions, the signal-to-noise ratio is greater than required. This is illustrated in Fig. 16 where location C represents the position where least optical power is received with the particular satellite LED array. In Fig. 18, the total satellite power P_s is shown as a function of the room size S for the three different satellite LED arrays. The upper-bound applies to the nondirectional case with all photosensitive surfaces parallel to the ceiling, whereas the lower bound applies for the semidirectional case. The smooth curve indicates the theoretical minimum power P_{so} if the optical radiation were available in the form of a plane wave with normal incidence and an aperture corresponding to the floor area $S \times S$, equation (5). The increased power demand P_s with respect to P_{so} is explained by a reflecting surface (walls and ceiling) larger than the floor area, nonuniform radiant emittance, and absorption. However, the satellite power approximately follows the theoretical square law if the LED arrays are adequately adapted to the room geometry. In practice, the satellite power calculated should be multiplied with a safety factor allowing for temporary or permanent partial obstruction of the individual FOV's, aging of the LED's, optical-filter losses, and receiver imperfections.

Alternatively, Fig. 19 shows the bit rates achievable as a function of the room size, given a total satellite power of 1 W including a safety factor of 5. It is apparent that for large rooms, an excessive power demand is more likely to be the limiting factor than signal dispersion due to multiple path propagation.

D. Optical Terminal Power

We shall now discuss the terminal-power requirements. In principle, to form a totally connected network, the same power

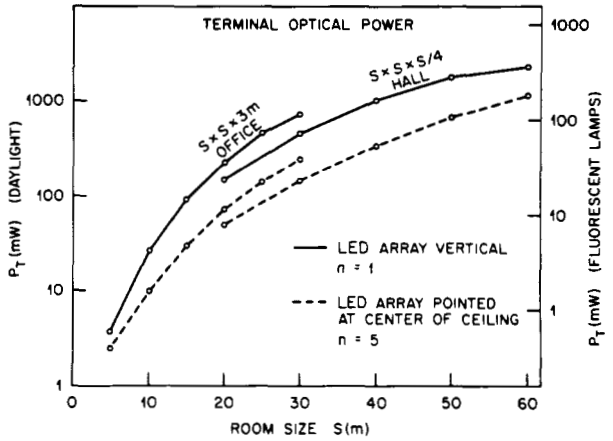

Fig. 20. Terminal optical power as a function of room size and geometry. Transmission speed 64 kbit/s.

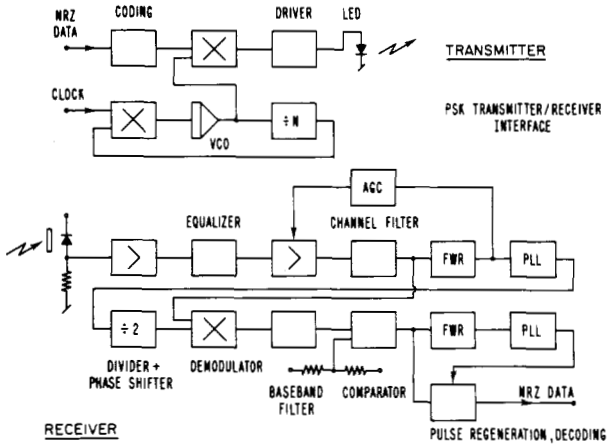

Fig. 21. Block diagram of the PSK transmitter-receiver interface.

as for the satellite is needed. However, the terminals are randomly located within the room and each terminal would therefore require an individual optical-source array to evenly disperse the radiant power to the environment. In the interest of a simple LED array at the terminal interface, it is favorable to establish a dedicated channel from each terminal to the satellite only. This approach requires different carrier frequencies for the up- and downlinks if full duplex operation is desired. Fig. 20 shows calculated results of the maximum terminal power required as a function of the room size. The transmission speed is again 64 kbit/s, and communication is assumed between a terminal located in a corner and the satellite located centrally. The satellite photodetector has a hemispherical receiver characteristic with an effective projected area $A_R = 1$ cm^2. With a cosine law characteristic (plane photosensitive area) the projected area for radiation incident from distant terminals is smaller, resulting in a lower signal-to-noise ratio. The isotropic receiver characteristics can be approximated by photodiodes resting on the faces of a tetrahedron. Fig. 20 shows both the nondirectional case with the LED axis normal to the ceiling and a semidirectional case. For larger values of n (narrower radiation lobe) and with the LED tilted towards the center of the ceiling, a further reduction of the terminal power can be achieved at the expense of a higher degree of directionality.

E. Discussion

The previous examples have shown that efficient illumination may be achieved and that the optical power received is quite insensitive to the angular orientation of the photodiodes. The dynamic range of the receiver circuit required to cope with the signal-power variation over the floor area is less than that for fiber-optic receivers having to adapt to different fiber lengths. So far, we have assumed that the entire floor area is to be provided with the signal carrier, but diffuse spotlights serving a local cluster in an otherwise large hall may also be considered. To extend the range, for instance in a large in-house plant, several distributed satellites operating at different carrier frequencies to avoid mutual interference, may be employed. In practice, a high level of ambient light is found near windows, whereas the interior of large rooms is comparatively dark or fluorescent lighting with a lower infrared portion prevails.

In the interest of an economical use of optical signal power in large rooms, the signal-to-ambient-light-noise ratio should be kept constant. This calls for a modular construction of the optical satellite and terminal interfaces. The basic transmitter and receiver circuits of both types of interfaces remain the same, but individual modules consisting of an LED driver and flexible LED array may be added to adapt the optical system to the various range, geometry, and ambient-light conditions. In modern buildings infrared-reflecting window panes are often installed to save energy for air conditioning and to provide a pleasant working climate. Transmission of incident daylight in the near-infrared region is thus reduced by up to 75 percent which represents a further gain in the signal-to-noise ratio.

The simulations were performed for a relatively well-defined reflecting environment. Production plants are often housed in a complex structural environment where the model described can only give the coarse features. Finer details of the signal-power distribution should be obtained from field tests.

A somewhat speculative thought is the use of laser diodes instead of LED's. The narrow source linewidth would allow the use of narrow-band optical interference filters offering a greatly reduced shot-noise level, and hence less signal power, depending on the spectrum of the ambient light. Furthermore, additional separate channels may be gained by using different optical wavelengths. An optical system to disperse the laser radiation to a safe level would be needed.

V. Experimental Transmitter-Receiver Interface

In this section, we describe an experimental PSK transmitter-receiver interface operating at a channel transmission speed of 64 kbit/s. The use of a modulated carrier allows the signal spectrum to be shifted away from the spectrum of ambient-light fluctuations. Furthermore, separate channels for the up- and downlinks, may be provided. Fluorescent lamps, for instance, exhibit a spectrum reaching as far as 50 kHz. The carrier frequency should, therefore, be higher than a few hundred kHz but less than a few MHz, depending on room size, to avoid phase distortions due to multipath distortion. The block diagram of the transmitter-receiver interface is shown in Fig. 21. At both ends of the interface, data are available in NRZ form. At the transmitter side, data from the terminal in NRZ form are first converted to RZ form. We have chosen diphase coding which provides easy clock extraction at the receiver end. As an alternative, scrambling can be used.

A PLL circuit synchronizes the carrier frequency with the clock frequency where the carrier is a multiple N of the clock

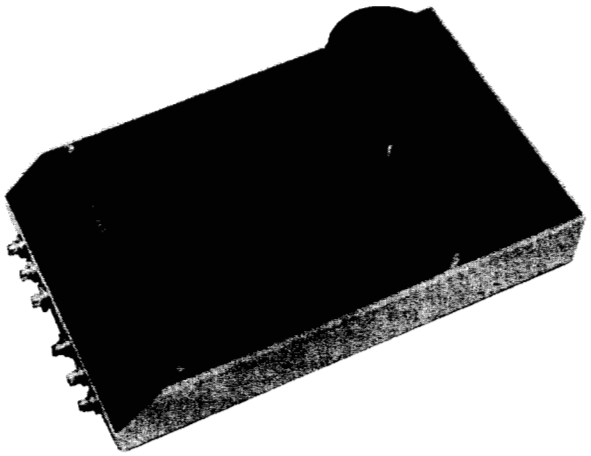

Fig. 22. Packaged 64-kbit/s PSK terminal transmitter-receiver interface.

frequency. The carrier is then keyed with the RZ data, and the resulting PSK signal is amplified to drive the LED array. On the receiver side the incoming signal is equalized after distortion by the photodiode capacitance and bias resistance. The channel filter selects the appropriate carrier-frequency band, and an automatic gain control keeps the signal at a constant level. The carrier is recovered with a PLL circuit, and after subsequent multiplication with the PSK signal, the baseband signal is obtained. Clock extraction is achieved with a second PLL circuit, and finally, pulse regeneration and conversion to NRZ form follow. Fig. 22 shows the packaged transmitter-receiver interface. The LED array consists of ten LD 271 diodes in series with an average optical radiant output power of 100 mW. An investigation has shown that emitted radiation from this diode type poses no safety hazard for the eyes [15].

The carrier frequency is 256 kHz, and with $N = 4$, the corresponding channel transmission speed is 64 kbit/s. The photodiode array consists of 9 BPW 34 diodes connected in parallel forming a total area of 0.67 cm^2. The transmission range between these terminal interfaces is 10–20 m depending on ambient-light conditions.

We have measured the stationary transmission error probability under an ambient-light environment of 380 Lux to values up to 10^{-7}. No interference arising from fluorescent lamps was detected. However, during switching-on of fluorescent lamps, the error probability may rise to approximately 10^{-3}. This period of increased error probability occurs only during the ignition phase of the fluorescent lamp and is typically shorter than 100 ms. The effect depends on intensity, proximity, and type of fluorescent lamp. With higher carrier frequencies, this effect is expected to be reduced or even eliminated. But considering the relative rarity of switching-on events per day, these short periods of increased error probability may not pose a problem.

Fig. 23 shows a prototype of the satellite interface. Up to eight flexible spotlights of 100-mW optical power each may be added to adapt the radiation pattern to the environment.

VI. Conclusions

We have analyzed the physical aspects of the diffuse optical channel and demonstrated technical feasibility. With the wireless transmission scheme great flexibility in terminal arrangement may be achieved. An experimental PCM baseband link and a PSK link, operating at 125 kbit/s and 64 kbit/s, respectively, have been built. The channel is suitable for low to medium speed transmission at low error rates and free from EMI.

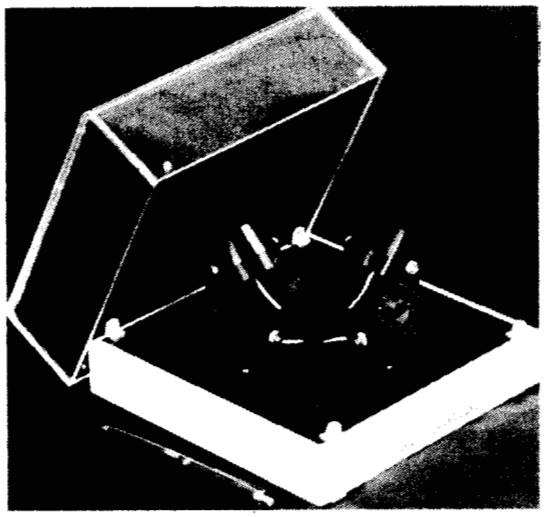

(a)

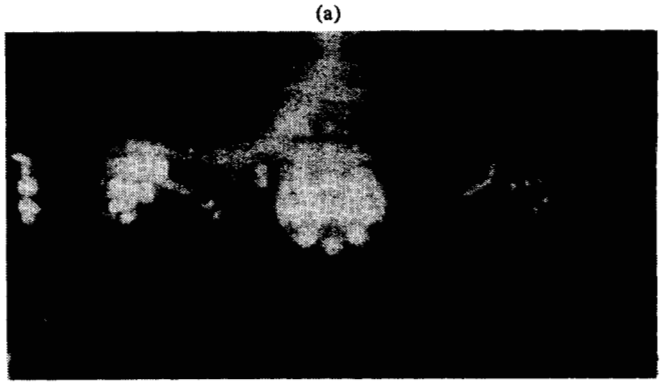

(b)

Fig. 23. (a) Packaged satellite interface. The plexiglass cover is transparent for infrared radiation. (b) Packaged satellite interface. Image convertor photograph. Each LED-array spotlight emits 100-mW average optical power.

With present low-cost state-of-the-art LED's, the maximum transmission speed is around 100 kbit/s due to the limited modulation capability of the LED. Higher transmission speeds up to 1 Mbit/s appear feasible if increased optical power raises no objection.

There is scope for improving the performance and reducing the cost of the satellite and terminal interfaces. Current trends indicate a decrease of hardware costs for optical components and circuitry, whereas costs of copper cables and labor for pulling cables are not likely to be reduced. Expenditure for fiber optics is still relatively high and the present state of development favors individual point-to-point links rather than distributed systems with a large population of users. There is, therefore, a challenge in identifying new applications of local-area networks where the wireless optical link can offer distinct advantages.

Acknowledgment

We should like to express our gratitude to H. R. Müller, P. Vettiger, and A. H. Frei for the help received and continuous support and encouragement during the course of the project.

References

[1] D. J. Farber and K. C. Larson, "The system architecture of the distributed computer system—The communication system," presented at The Polytechnic Inst. Brooklyn Symp. Computer

Networks, Brooklyn, NY, Apr. 1972.
[2] R. Metcalfe and D. R. Boggs, "Ethernet: Distributed packet switching for local computer networks," presented at Xerox Palo Alto Research Center, Palo Alto, CA, Nov. 1975.
[3] A. G. Fraser, "Spider—An experimental data communications system," in *1974 Int. Commun. Conf.*, pp. 21F-1, 10.
[4] F. R. Gfeller, H. R. Müller, and P. Vettiger, "Infrared communication for in-house applications," presented at IEEE COMPCON '78 (Washington DC), Sept. 5-8, 1979.
[5] L. G. Roberts, "Extension of packet communication technology to a hand-held personal terminal," in *Proc. AFIPS Spring Joint Comp. Conf.*, vol. 40, pp. 295-298, 1972.
[6] R. Bryan, "Research in micro-terminal development and network end-to-end error recovery," California University Advanced Research Projects Agency Defense Supply Service, AD/A-006589, Feb. 1975.
[7] L. Kleinrock and S. S. Lam, "Packet switching in a multi-access broadcast channel: Performance evaluation," *IEEE Trans. Commun.*, vol. COM-23, Apr. 1975.
[8] R. Winston, "Light collection within the framework of geometrical optics," *J. Opt. Soc. Amer.*, vol. 60, pp. 245-247, Feb. 1970.
[9] A. Rabl, "Comparison of solar concentrators," *Solar Energy*, vol. 18, pp. 93-111, 1976.
[10] R. Knauer, "Tonübertragung und Fernsteuerverfahren mit Infrarot," Siemens A. G., München, Germany, Bereich Bauelemente Vertrieb, Tech. Schrift.
[11] J. E. Goell, "Input amplifiers of optical PCM receivers," *Bell Syst. Tech. J.*, vol. 53, pp. 1771-1793, Nov. 1974.
[12] S. D. Personick, "Receiver design for digital fiber optic communication systems," *Bell Syst. Tech. J.*, vol. 52, pp. 843-874, 1973.
[13] D. B. MuKunda, "FET noise sources and their effects on amplifier performance at low frequencies," *IEEE Trans. Electron Devices*, vol. ED-19, pp. 338-348, Mar. 1972.
[14] P. Bocker, *Datenübertragung Band I.* New York: Springer, 1976, pp. 129-133.
[15] Kuny, "Augenschädigung durch Infrarot-Strahler," Siemens A. G., Bericht. Aktenvermerk 150 000 8.71 2181.

Transform Approach to Electromagnetic Scattering

RAJ MITTRA, FELLOW, IEEE, WAI LEE KO, MEMBER, IEEE, AND YAHYA RAHMAT-SAMII, MEMBER, IEEE

Invited Paper

Abstract—In this paper, we present a comprehensive review of the Fourier transform technique as applied to the problem of high-frequency scattering and introduce the concepts of the spectral theory of diffraction (STD). In contrast to the more commonly employed ray-optical method for high-frequency scattering, viz. the geometrical theory of diffraction (GTD), the STD approach interprets the scattered field as the spectrum, or the Fourier transform of the induced current on the scatterer. Such an interpretation offers several important advantages: uniform nature of representation, capacity to improve and extend the ray-optical formulas in a systematic manner, and convenient accuracy tests for the results. Methods for combining integral equation methods with the Galerkin procedure and asymptotic techniques in the transform domain are described, and representative examples illustrating the application of the spectral approach are included.

NOMENCLATURE

STD	Spectral theory of diffraction.
UTD	Uniform theory of diffraction.
UAT	Uniform asymptotic theory.
u^i	Incident field.
u^s	Scattered field.
u^t	Total field.
E	Electric field.
H	Magnetic field.
J	Induced electric current.
F	Fourier transform operator.
F^{-1}	Inverse Fourier transform operator.
$\tilde{U}$	Transformed function.
$\tilde{J}$	Transformed function.
X	Spectral diffraction coefficient.
H^d	Edge diffracted field.
H^P	Physical optics field.
H^g	Geometrical optics field.
H_1	Field of edge 1.
H_2	Field of edge 2.
F	Fresnel function.
$\hat{F}$	Asymptotic term of Fresnel function.
J^b	Physical optics current.
J^{tr}	Truncated physical optics current.
J^1	Induced current on a semi-infinite half-plane.
H^D	Diffracted field in UTD formulation.
θ	Step function in Section III.
θ	Truncation operator in Section IV.
$\hat{\theta}$	Complimentary operator.
$\bar{\bar{G}}$	Dyadic Green's function.
$\tilde{J}_p$	Basis function.
$\tilde{W}_q$	Testing function.

Manuscript received December 4, 1978; revised July 5, 1979.
This work was supported in part by Joint Services Electronics Projects under Grant N00014-79-C-0424, and in part by Office of Naval Research under Grant N00014-75-C-0293.

R. Mitra and W. L. Ko are with the Electromagnetics Laboratory, Department of Electrical Engineering, University of Illinois, Urbana, IL 61801.
Y. Rahmat-Samii is with the Jet Propulsion Laboratory, California Institute of Technology, Pasadena, CA 91103.

0018-9219/79/1100-1486$00.75

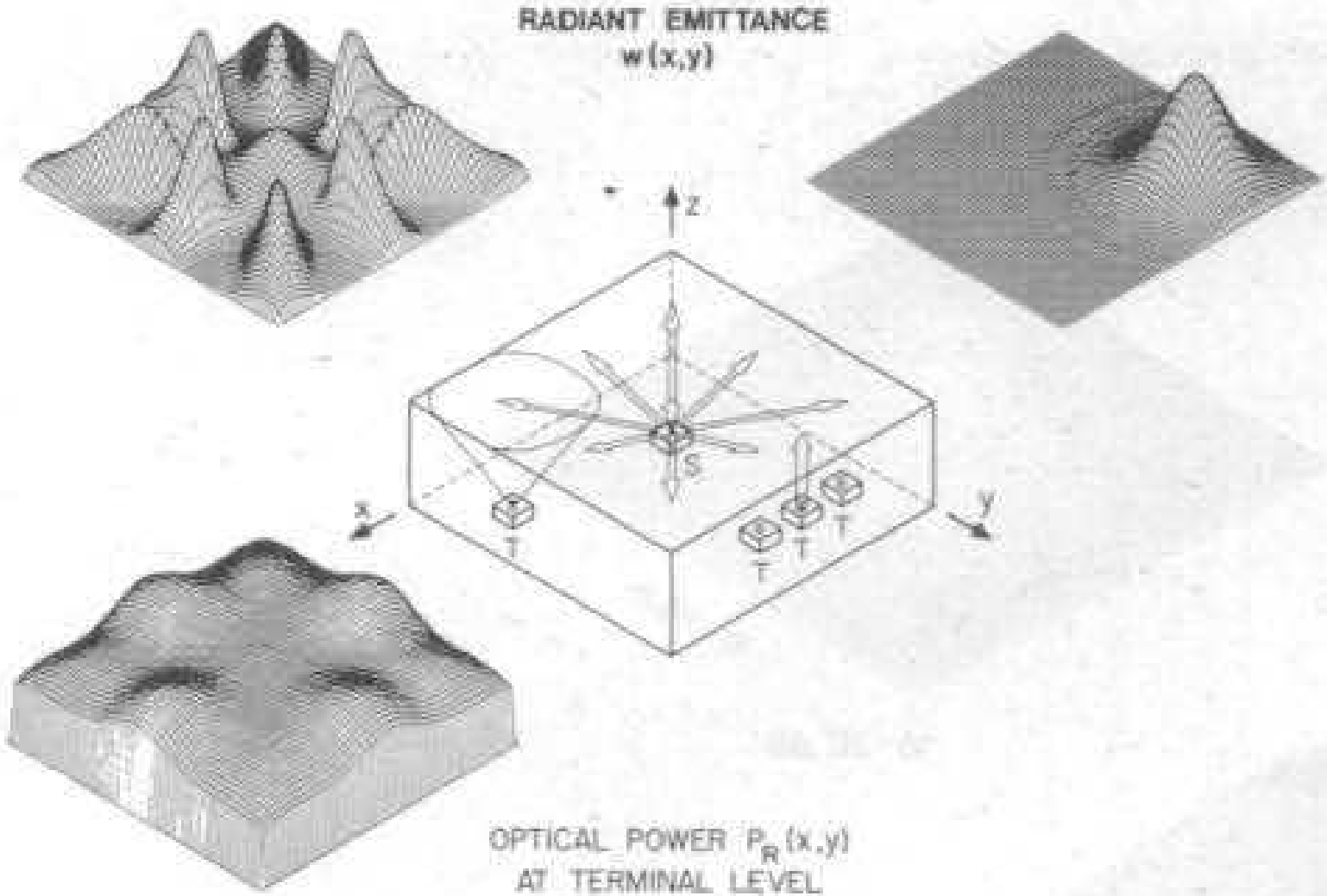

Fig. 12. Distribution of diffuse optical radiation in an office room environment. The plot in the upper-left corner shows the radiant emittance of the ceiling as produced by the satellite Sat. with a source array of nine LED's. The upper-right plot shows the radiant emittance produced by a terminal T with a Lambertian LED. The lower plot indicates the resulting received optical power (downlink) as a function of the terminal position. $S = 10$ m, $H = 3$ m, FOV = 90°, nondirectional case.

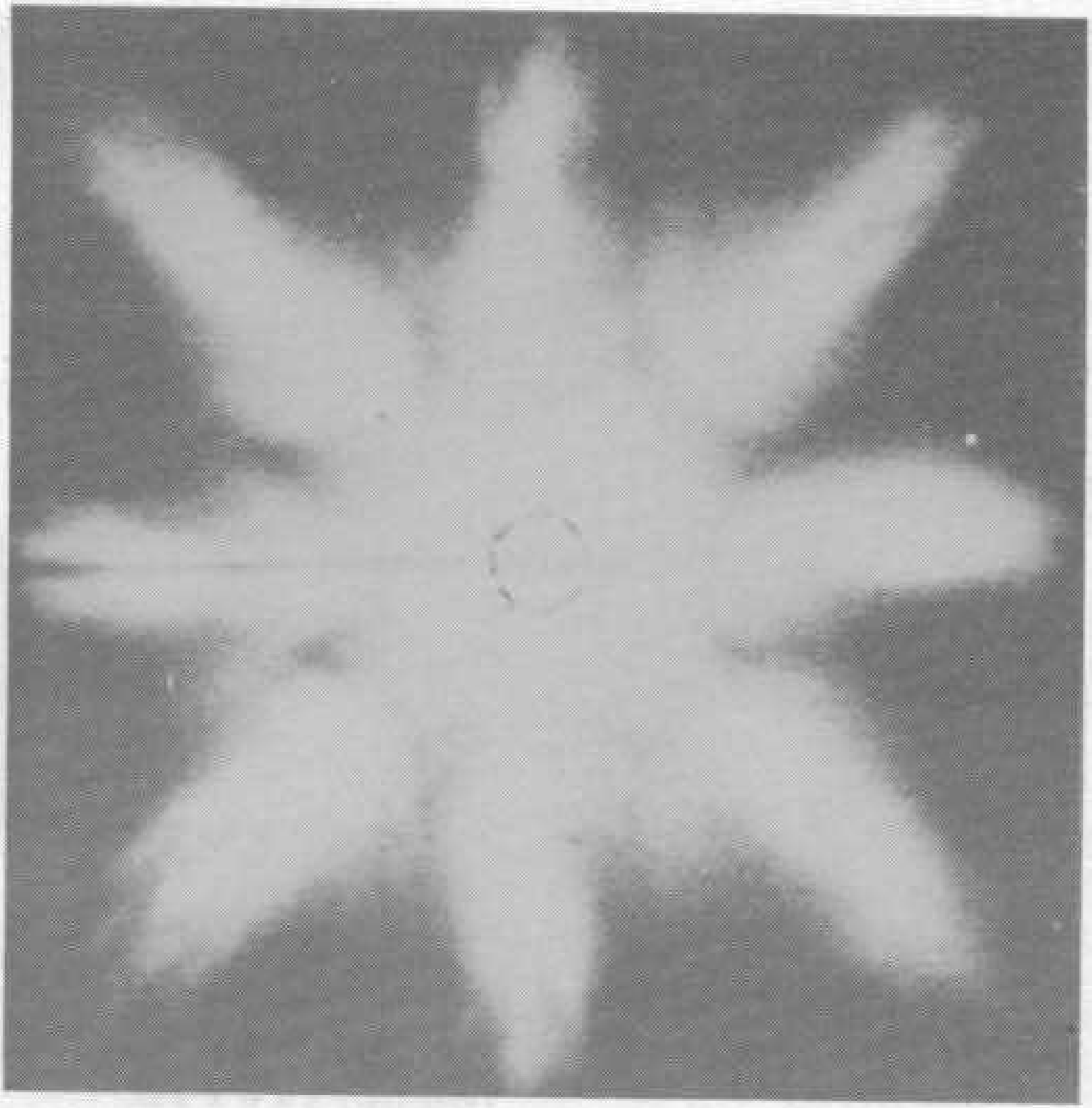

Fig. 13. Infrared spotlight pattern on diffusely reflecting surface. Image convertor photograph. The source consists of nine LED arrays. The irregularities of the individual LED radiation lobes are caused by manufacturing tolerances.

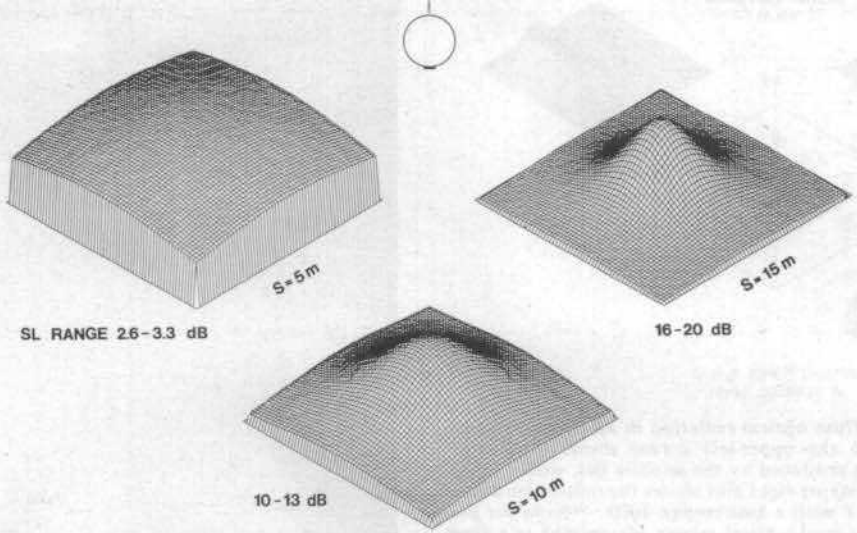

Fig. 14. Small office room. Received optical power as a function of terminal position. The dB figures indicate the encountered signal power variations for the semi- and nondirectional cases, respectively. The symbol indicates the Lambertian source. Plots refer to photodiodes in semidirectional orientation. FOV = 90°; room geometry $S \times S \times 3$ m.

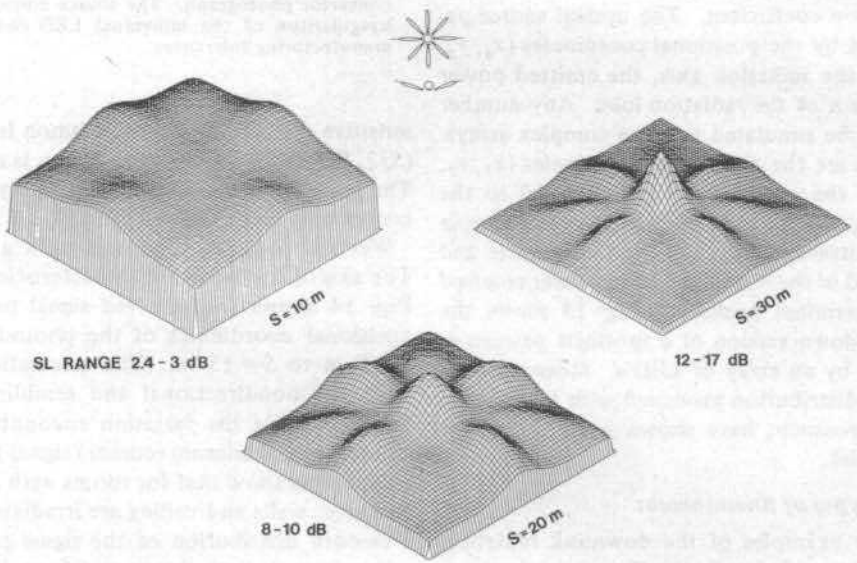

Fig. 15. Large office room. Received optical power as a function of terminal position. The dB figures indicate the encountered signal power variations for the semi- and nondirectional cases, respectively. The satellite source consists of eight LED's with $n = 100$, and one LED with $n = 1$. The location of the window front ($S = 1$) corresponds to the side marked with the room size S. Plots refer to photodiodes in nondirectional orientation. FOV = 90°; room geometry $S \times S \times 3$ m.

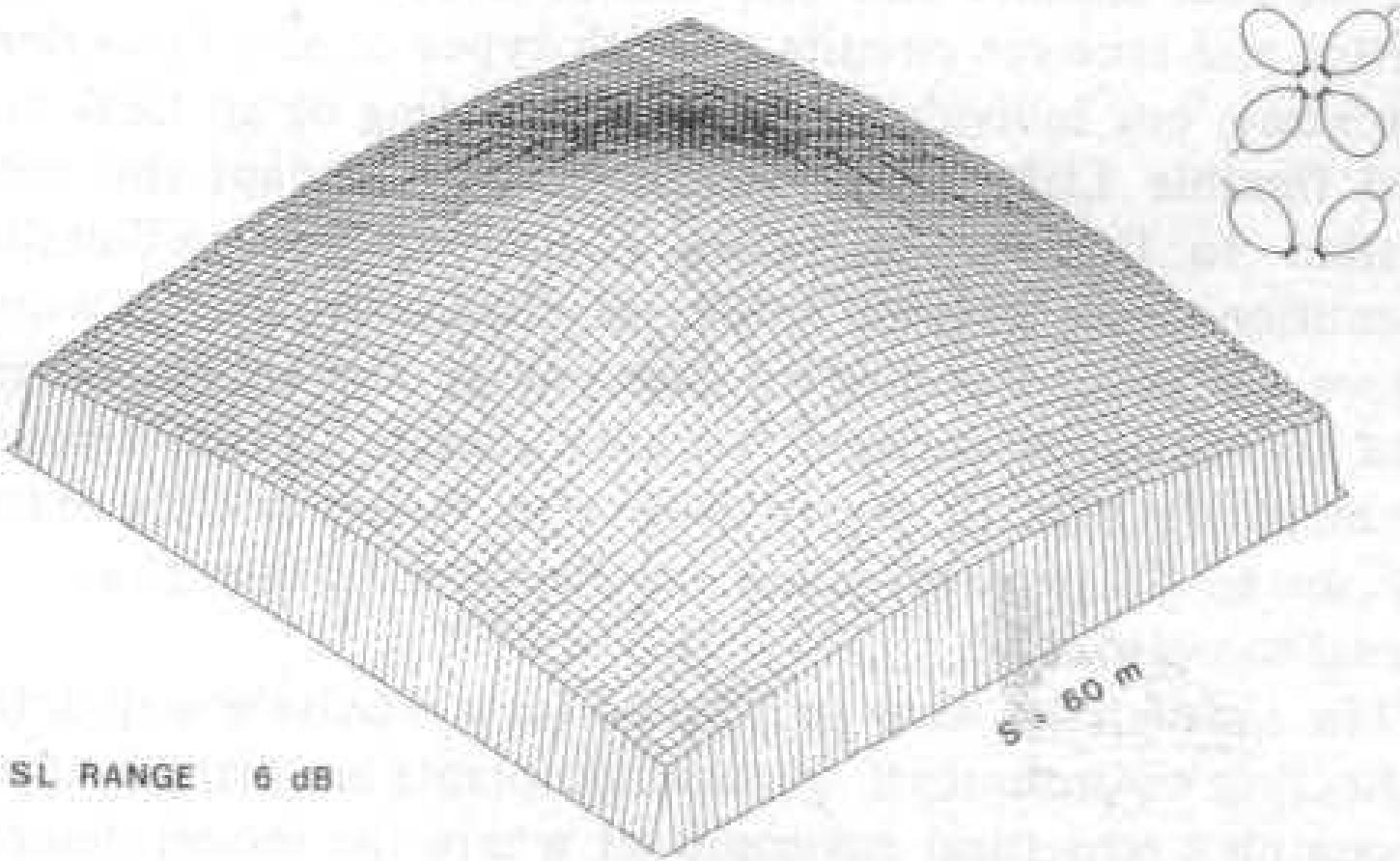

Fig. 17. Hall. Received optical power as a function of terminal position. There is little difference between semi- and nondirectional photodiode orientation. Satellite source consists of four LED's with $n = 3$. FOV = 90°; room geometry $S \times S \times S/4$.

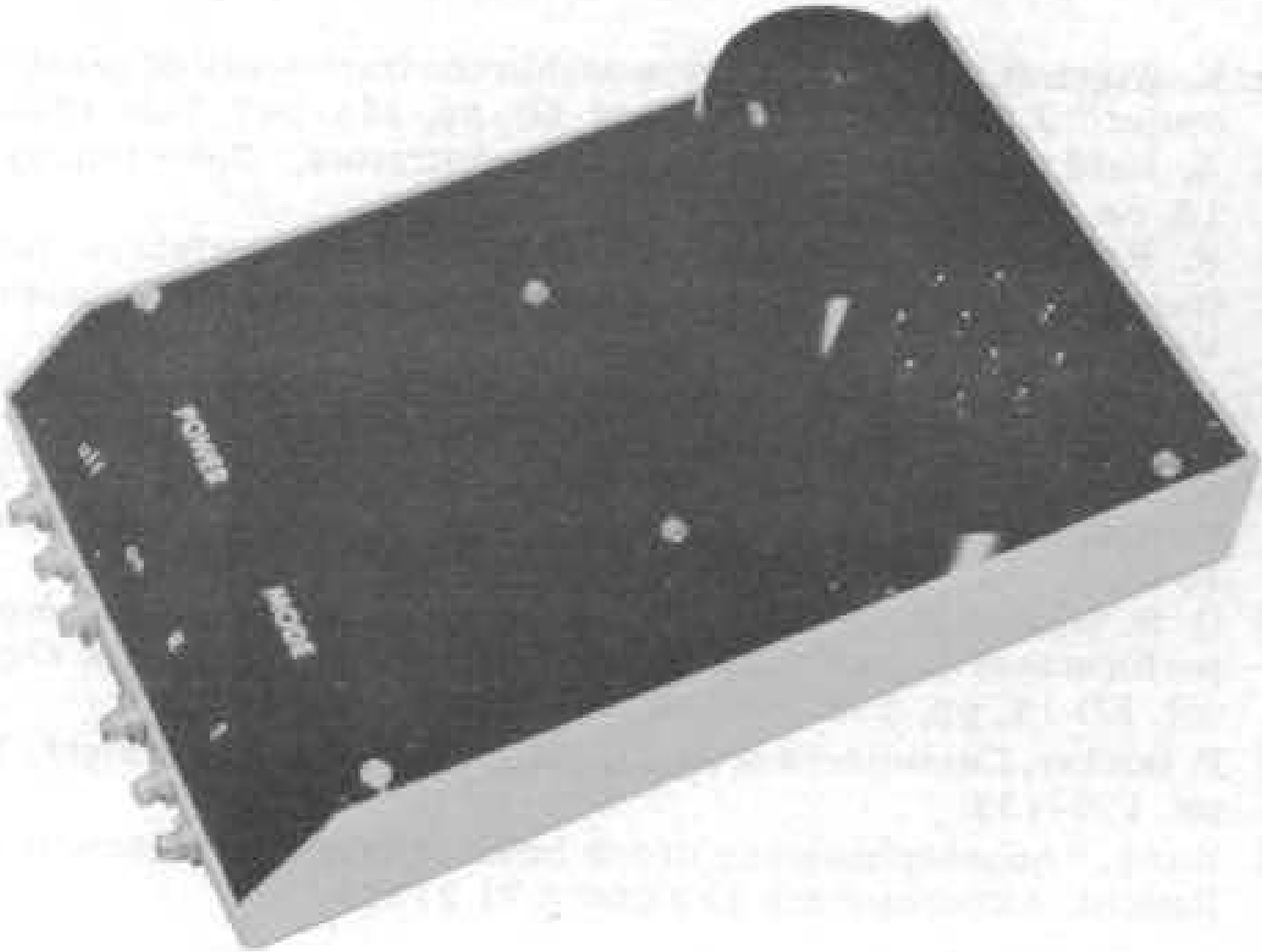

Fig. 22. Packaged 64-kbit/s PSK terminal transmitter-receiver interface.

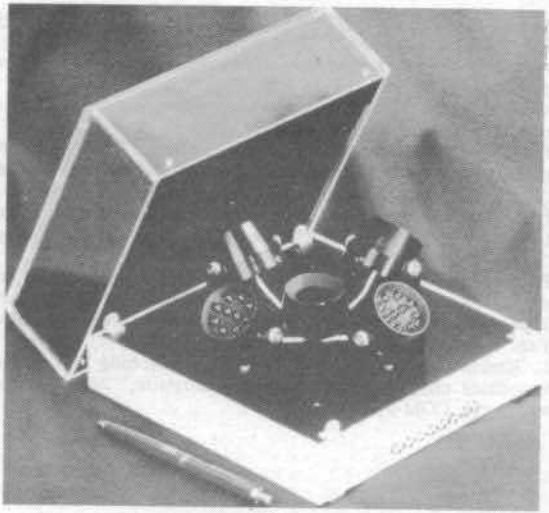

(a)

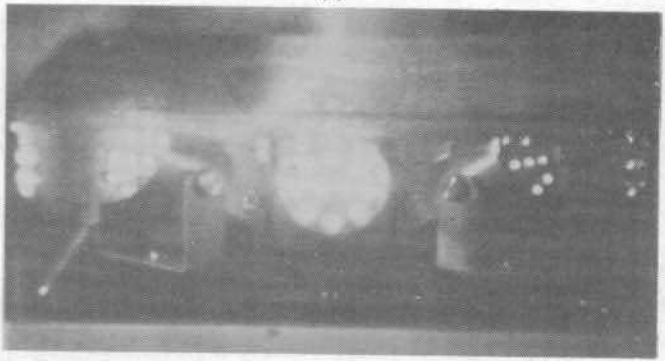

(b)

Fig. 23. (a) Packaged satellite interface. The plexiglass cover is transparent for infrared radiation. (b) Packaged satellite interface. Image convertor photograph. Each LED-array spotlight emits 100-mW average optical power.